Received: 25 October 2021 | Revised: 18 January 2022 | Accepted: 8 February 2022

DOI: 10.1111/bph.15821

RESEARCH ARTICLE

Mechanistic modelling of enzyme-restoration effects of new recombinant liver-targeted proteins in acute intermittent porphyria

Diego Vera-Yunca[1,2] | Karol M. Córdoba[2,3] | Zinnia P. Parra-Guillen[1,2] | Daniel Jericó[2,3] | Antonio Fontanellas[2,3,4] | Iñaki F. Trocóniz[1,2]

[1]Pharmacometrics & Systems Pharmacology, Department of Pharmaceutical Technology and Chemistry, School of Pharmacy and Nutrition, University of Navarra, Pamplona, Spain

[2]IdiSNA, Navarra Institute for Health Research, Pamplona, Spain

[3]Hepatology Program, Center for Applied Medical Research (CIMA), University of Navarra, Pamplona, Spain

[4]Centro de Investigación Biomédica en Red de Enfermedades Hepáticas y Digestivas (CIBERehd), Instituto de Salud Carlos III, Madrid, Spain

Correspondence
Iñaki F. Trocóniz, Pharmacometrics and Systems Pharmacology Group (http://www.unav.edu/psp), Department of Pharmaceutical Technology and Chemistry, School of Pharmacy and Nutrition, University of Navarra, Calle Irunlarrea 1, 31008 Pamplona, Spain.
Email: itroconiz@unav.es

Funding information
Fundación FEDER para la investigación de enfermedades raras, Grant/Award Number: F19-010-V; Instituto de Salud Carlos III, Grant/Award Numbers: PFIS, FI19/00014, PI18/00860, PI21/00546; Ministerio de Educación y Formación Profesional, Grant/Award Number: FPU, FPU18/01165; Spanish Fundación Mutua Madrileña

Background and Purpose: Acute intermittent porphyria (AIP) is a rare disease caused by a genetic mutation in the hepatic activity of the porphobilinogen-deaminase. We aimed to develop a mechanistic model of the enzymatic restoration effects of a novel therapy based on the administration of different formulations of recombinant human-PBGD (rhPBGD) linked to the ApoAI lipoprotein. This fusion protein circulates in blood, incorporating into HDL and penetrating hepatocytes.

Experimental Approach: Single i.v. dose of different formulations of rhPBGD linked to ApoAI were administered to AIP mice in which a porphyric attack was triggered by i.p. phenobarbital. Data consist on 24 h urine excreted amounts of heme precursors, 5-aminolevulinic acid (ALA), PBG and total porphyrins that were analysed using non-linear mixed-effects analysis.

Key Results: The mechanistic model successfully characterized over time the amounts excreted in urine of the three heme precursors for different formulations of rhPBGD and unravelled several mechanisms in the heme pathway, such as the regulation in ALA synthesis by heme. Treatment with rhPBGD formulations restored PBGD activity, increasing up to 51 times the value of the rate of tPOR formation estimated from baseline. Model-based simulations showed that several formulation prototypes provided efficient protective effects when administered up to 1 week prior to the occurrence of the AIP attack.

Conclusion and Implications: The model developed had excellent performance over a range of doses and formulation type. This mechanistic model warrants use beyond ApoAI-conjugates and represents a useful tool towards more efficient drug treatments of other enzymopenias as well as for acute intermittent porphyria.

KEYWORDS
acute intermittent porphyria, AIP, mechanistic, modelling, porphobilinogen deaminase

Abbreviations: ALA, 5-aminolevulinic acid; ALAS, 5-aminolevulinic acid synthase; AIP, acute intermittent porphyria; ApoAI, apolipoprotein AI; PBG, porphobilinogen; PBGD, porphobilinogen deaminase; Phe, phenobarbital; tPOR, total porphyrins; URO, uroporphyrin; Vmax, maximum rate of PBG conversion; γHeme, parameter that regulates the magnitude of heme inhibition on hepatic ALA synthesis; γPBGD, parameter modulating the effect of the excess of PBG on the transit between hepatic ALA and hepatic PBG.

1 | INTRODUCTION

Porphyrias are a group of metabolic diseases caused by genetic mutations in enzymes involved in the heme biosynthesis pathway. The heme biosynthesis metabolic route starts with the conversion of succinyl-CoA and glycine into **5-aminolevulinic acid (ALA)** by the ALA synthase (ALAS, EC 2.3.1.37) enzyme. This step is the rate-limiting factor of the entire pathway and it is tightly controlled by the free heme pool inside the cell. High intracellular heme levels decrease the transcription of the ALAS gene (*ALAS1*) as well as its translation and its entrance to the mitochondria (Phillips, 2019).

More specifically, acute intermittent porphyria (AIP; MIM 17600) (Karim et al., 2015) is caused by a loss-of-function mutation in the porphobilinogen (PBG) deaminase (D) gene (*HMBS*), thus reducing the catalytic activity of the third enzyme of the heme synthesis pathway. AIP is characterized by disabling neurovisceral attacks and chronic disease symptoms, such as non-focal abdominal pain often accompanied by nausea, vomiting, constipation, hyponatremia, hypertension, psychological and neurological symptoms that can lead to respiratory paralysis and death (Karim et al., 2015).

Overall PBGD gene (*HMBS*) mutation prevalence is 1 in 1786 individuals, although the clinical penetrance of the disease is very low (<1% of the patients with the mutation) (Chen et al., 2016). Acute neurovisceral attack can be triggered by factors including medication and other chemicals, certain steroids hormones, stress, infection, caloric deprivation and rapid weight loss. Those triggers mainly consist of situations in which intracellular heme levels are decreased in the liver (e.g. an increase in **cytochrome P450** production due to drugs or hormones, more heme oxygenase activity) (Thunell et al., 2007). Furthermore, hepatic ALAS gene, expression can also be directly induced by certain chemicals, such as barbiturates (Kakizaki et al., 2003) or by fasting (Handschin et al., 2005).

Any of the above mentioned factors could precipitate an acute porphyric attack in patients with AIP. For example, the hepatic heme pathway is activated by a combination of intracellular heme reduction and ALAS direct induction. The activation of the heme pathway and the impaired PBG deaminase catalytic activity results in an accumulation of porphobilinogen (PBG) and 5-aminolevulinic acid (ALA) that reach systemic circulation and then excreted in urine (Wang, 2021).

The standard-of-care therapy for AIP is hemin (Stein et al., 2013), an analogue of heme that is administered during the acute attacks to replenish the heme deposits in the liver, thus inhibiting the heme biosynthesis pathway. However, hemin requires hospitalization has it has to be given intravenously. Patients with chronic acute attacks develop side effects as a consequence of frequent hemin administrations such as central vein damage and iron overload, which can lead to chronic inflammatory response (Schmitt et al., 2018) and hepatic damage (Zhao et al., 2020). Indeed, hemin administration induces the activity of the key enzyme of heme catabolism, the heme oxygenase, resulting in the reduction of the regulatory heme concentration in the cell. This situation induces a feedback mechanism to restore regulatory heme in the cells through the activation of ALAS, which reduced the therapeutic efficacy of hemin administration (Dover et al., 1993).

What is already known

- Recombinant human PBGD is a potential alternative to hemin for treatment of acute intermittent porphyria.

What does this study add

- *In vivo* mechanistic characterization of the enzymatic restoration effects based on recombinant human ApoAI-PBGD proteins.
- A tool to explore *in silico* scenarios involving different dosing regimens of the ApoAI-conjugated molecule.

What is the clinical significance

- This framework can used to develop treatments for acute intermittent porphyria and other enzymopenias.

As an alternative to hemin treatment, several innovative therapies are currently being developed including a small interference RNA targeting the ALAS1 mRNA (Syed, 2021), as well as an mRNA encoding human PBGD (Jiang et al., 2018). Another innovative therapeutic approach is based on a recombinant fusion protein comprised of the human PBGD (hPBGD) enzyme and the apolipoprotein AI (ApoAI), where the addition of the ApoAI protein helps to direct PBGD to the liver in order to increase hepatic PBGD activity and residence time (Córdoba et al., 2022).

The fact that AIP is a rare disease hampers the development of new therapeutics due to limited knowledge of the disease pathophysiology and lack of eligible patients for clinical trials (Gopal-Srivastava & Kaufmann, 2017). In that particular context, the building of computational multiscale models which merge treatment and disease features mechanistically through the integration of data from multiple sources represents an appealing approach to increase disease understanding and to accelerate discovery and development (Huang et al., 2013) of new therapeutics.

To the best of our knowledge, modelling efforts focused on AIP are still very scarce. Vera-Yunca et al. (2019) developed recently a semi-mechanistic model capturing the dynamics of the changes in the heme pathway as the result of the AIP attacks triggered by the porphyrinogenic drug **phenobarbital** through the time profiles of ALA, PBG and total porphyrins (tPOR) excreted in urine. In that model, some of the main regulatory mechanisms in the heme pathway could not be identified as the experimental system perturbation was limited. Still, it constituted the disease model platform leveraging multiscale data gathered during the preclinical development of mRNA therapies (Parra-Guillen et al., 2020). This allowed the extrapolation of hPBGD

effect to humans by simulating different dose levels and single or multiple dose administrations.

In this study, the previous disease model has been expanded, increasing its mechanistic structure by including data under treatment with different recombinant fusion proteins composed of the hPBGD linked to ApoAI administered at several i.v. dose levels (Córdoba et al., 2022). The integration of all the available experimental data warranted quantitative characterization of main regulatory mechanisms of the heme pathway and allowed to establish a robust tool to be considered within the model-based drug discovery and development (MID3) paradigm (Marshall et al., 2016). As a corollary, the model was externally validated in an experimental setting where the treatment was given as a subcutaneous (s.c.) injection, which supports its usefulness.

2 | METHODS

2.1 | Experimental protocol

2.1.1 | Available data and animal model

Data used to build the heme pathway mechanistic computational model were provided by the Center for Applied Medical Research (CIMA), University of Navarra. Two kinds of longitudinal measurements were obtained, PBGD enzymatic activity from *in vitro* experiments and heme precursor (ALA, PBG and total porphyrins [tPOR]) amounts in urine of either control or treated animals.

The animal model used in this work was obtained from male C57BL (RRID:MGI:5657800) mice, by crossbreeding T1(C57BL/6 $^{pbgdtm1(neo)Uam}$) and T2 (C57BL/6 $^{pbgdtm2(neo)Uam}$) mouse strains as described elsewhere (Parra-Guillen et al., 2020). The result is a mouse strain with only 30% of its original normal PBGD activity (AIP mice) that reproduced phenotypical and biochemical features of patients with AIP. Animal studies are reported in compliance with the ARRIVE guidelines (Percie du Sert et al., 2020) and with the recommendations made by the *British Journal of Pharmacology* (Lilley et al., 2020).

To evaluate the therapeutic efficacy of recombinant human PBGD (rhPBGD) proteins conjugated to ApoAI, we designed pharmacokinetic studies with the recombinant ApoAI conjugated proteins after i.v. or s.c. administration in female AIP mice (10–20 weeks old). We determined serum PBGD activity at different time points. For pharmacodynamic studies, male AIP mice (10–16 weeks old) challenged with phenobarbital were i.v. or s.c. injected with, rhPBGD-ApoAI, rhApoAI-PBGD and human PBGD-I129M/N340S variant conjugated to ApoAI (rhApoAI-PBGDMS) to compare their short- and long-term efficacy in preventing acute porphyria attacks. For this purpose, ALA, PBG and tPOR urinary excretion were measured daily during the phenobarbital challenge. Experimental protocols were approved by the Ethics Committee of the University of Navarra (CEEA009-11 and CEEA048-15), according to European Council Guidelines. Figure S1 shows the experimental design for both kinds of studies.

2.1.2 | Synthesis of the rhPBGD molecules linked to the ApoAI lipoprotein

The rhPBGD molecules linked to the ApoAI lipoprotein were used to deliver the enzyme to the liver of AIP mice. Moreover, the link position in the rhPBGD protein (in either the amino or the carboxy terminus) was investigated to determine if it caused any differences in rhPBGD hepatic bioavailability, resulting in the rhPBGD-ApoAI and rhApoAI-PBGD fusion proteins. Besides, the substitution of two amino acids of the rhPBGD protein (rhPBGDMS) improved the catalytic function of the enzyme (Serrano-Mendioroz et al., 2018). This change, combined with the ApoAI lipoprotein, led to the rhApoAI-PBGDMS protein. The methodology used for the synthesis and the characterization of the three above ApoAI based formulations are described in detail elsewhere (Córdoba et al., 2022). The synthesis method of rhPBGD-ApoAI, rhApoAI-PBGD and rhApoAI-PBGDMS has changed over time and because of a significant percentage of protein aggregation that had to be reduced/abolished, which reduced the overall reaction efficiency. Further, the purification process that removed bacterial traces (such as LPSs) hampered the protein yield. The variable protein production made the final number of experimental animals used vary for each experiment.

2.1.3 | Serum PBGD enzymatic activity over time after a single PBGD intravenous dose

A total of 44 AIP mice received 60 nmol·kg^{-1} of either rhPBGD-ApoAI (n = 27), rhApoAI-PBGD (n = 9) or rhApoAI-PBGDMS (n = 8) as a single i.v. administration of 200 μl into the tail vein. Then, blood samples (434 samples in total) were taken at different times (5 min, 10 min, 20 min, 40 min, 60 min, 2 h, 4 h, 8 h, 24 h, 36 h, 48 h, 3 days, 4 days, 5 days and 6 days) and centrifuged to determine serum PBGD activity *in vitro*. The volume drawn at each time point was small (approximately 40-50 microliters), total extraction in the first 8 hours represents 16% of the total blood volume of a mouse of 25 g body weight. At the end of the first 8 h round and also after each daily draw, 1 ml of saline serum and a complex of vitamins and amino acids (Duphalyte® - Zoetis, Girona, Spain) were subcutaneously administered to replace fluids and prevent weakening of the animal. PBGD activity in serum was quantified measuring the conversion of PBG to uroporphyrin (URO). Briefly, 10 μl of serum were diluted with 15 μl phosphate buffer (obtained by adding a monobasic solution, NaH_2PO_4-$2H_2O$, to a dibasic solution, Na_2HPO_4-$2H_2O$, until pH 7.6 is reached), DTT, and Cl_2Mg; and pre-incubated with 200 μl of Tris–HCl 0.1 M (pH 8.1) for 3 min at 37°C. Then, the mixture was incubated in the dark with 25 μl PBG substrate 1 mM for 60 min at 37°C. The reaction was stopped with 1000 μl cold TCA 10% and the formed uroporphyrinogen I was oxidized to uroporphyrin after light exposure. Uroporphyrins were measured quantitatively in a PerkinElmer LS50B spectrofluorometer (PerkinElmer España S.L., Tres Cantos, Spain) with an excitation peak at 405 nm and window emission peak values between 550 and 660 nm. Results were expressed in terms of pmol uroporphyrin (URO) * μl serum^{-1} * h^{-1}.

2.1.4 | Heme precursor levels in urine after phenobarbital-induced recurrent acute attacks

To mimic acute porphyric attacksrepeated doses of phenobarbital, a drug that induces the heme pathway, was administered intraperitoneally (i.p.) to AIP mice in order to trigger the accumulation and excretion of heme precursors in urine. After each dose of phenobarbital, mice were housed in individual cages. Half of the cage was positioned on top of a thermal blanket for 4 h to avoid hypothermia (in case an animal is hot, it can move to the unheated area). After that time, mice were injected with 0.5 ml of warm saline to avoid dehydration and were placed in the metabolic cages to collect urine (from approximately 12 PM to 8 AM the next day). Four hours after the last dose, the rotarod, pain, step length and nerve conduction studies were performed. Porphyric animals showed signs of pain and motor troubles, but not wild type animals or AIP mice treated with specific therapies. AIP mice received four phenobarbital challenges starting at days 1, 8, 15 and 29. In each challenge, four increasing doses of phenobarbital were administered in intervals of 24 h (75, 80, 85 and 90 $mg \cdot kg^{-1}$). Exceptionally, a fifth dose of 90 $mg \cdot kg^{-1}$ was administered to AIP mice to confirm the protective effect of the administered protein. Between 10% and 15% of the animals did not conclude the study either due to death or because their general condition made it inadvisable to complete phenobarbital challenge protocol. Animals were randomly allocated into control and treated groups. Control AIP mice ($n = 22$) received only phenobarbital doses, whereas treated AIP mice were also administered either rhPBGD-ApoAI, rhApoAI-PBGD or rhApoAI-PBGDMS as a single i.v. dose at day 2. Several dose levels were tested: 300 ($n = 8$) and 600 ($n = 7$) $nmol \cdot kg^{-1}$ for rhPBGD-ApoAI and 300 $nmol \cdot kg^{-1}$ for rhApoAI-PBGD ($n = 7$) and rhApoAI-PBGDMS ($n = 6$). Total volume of urine excreted was collected daily during the acute attacks and the amount of heme precursors ALA (775 samples), PBG (778 samples) and tPOR (681 samples) was quantified as described elsewhere (Córdoba et al., 2022).

2.2 | Data analysis

Data and statistical analysis complied with the recommendations of the *British Journal of Pharmacology* on experimental design and analysis in pharmacology (Curtis et al., 2018). Three sequential steps were followed to develop an integrated mechanistic model capable to handle the data from any of the experimental conditions. First, the kinetics of the PBGD enzymatic activity measured in serum were characterized and used as a surrogate of the (unmeasured) PBGD systemic exposure. Then, the time course of the biomarkers in urine reflecting AIP triggered by phenobarbital were described based on the 24 h urinary excreted profiles of the biomarkers ALA, PBG and tPOR in mice not receiving active treatment. Finally, the 24 h urinary excreted profiles of the biomarkers from mice receiving both the injection of phenobarbital and PBGD formulations contributed to delineate the pharmacodynamic properties of exogenous PBGD.

In each of the aforementioned steps, all the available data were analysed simultaneously by following the population approach using NONMEM 7.4 (Beal et al., 2009) with the First Order Conditional Estimation (FOCE) with interaction method. All observations were logarithmically transformed for the analyses. Inter-animal variability in model parameters was modelled using an exponential model preventing negative values for the individual model parameters. The residual variability was described with an additive model in logarithmic scale.

2.2.1 | Model selection

Selection across competing models was performed in accordance with several criteria: (i) the log likelihood-ratio test in which a drop of 3.84 and 6.61 points in the minimum value of the objective function [approximately equal to $-2 \times$ log likelihood ($-2LL$)] between two nested model differing in one parameter is significant at the 5 and 1% levels, respectively. For non-nested models, the Bayesian Information Criterion was used instead; (ii) precision of the parameter estimates, expressed as the relative standard error (RSE) and calculated as the ratio between the standard error and the estimate of the parameter. Models with parameters associated with a relative standard error below 50% were considered acceptable; and (iii) visual inspection of the goodness-of-fit plots.

2.2.2 | Model evaluation

The selected models were evaluated using simulation-based model diagnostics such as prediction-corrected visual predictive checks (VPCs) (Phillips, 2019). One thousand studies with the same design characteristics as the original one were simulated. For each simulated study and time of measurement, the 2.5th, 50th and 97.5th percentiles of the simulated values were computed. Then the 95% confidence interval of the median was calculated and plotted together with the corresponding percentiles obtained from raw data. Besides, parameter precision was further assessed by performing either a non-parametric bootstrap (Efron, 1992) for the PBGD activity model or a log-likelihood profiling method (Sheiner, 1986) for the heme precursors model. The former technique used 1000 bootstrapped datasets and then fitted the model to these databases to obtain 95% confidence intervals (CI). The latter technique tested a range of different parameter values to observe changes in the $-2 \times$ log likelihood value, allowing us to compute 95% CI.

2.2.3 | Model exploration

The efficacy of different therapeutic scenarios including administration of PBGD at different times with respect to the beginning of the acute attack, different doses and schedules (300 $nmol \cdot kg^{-1}$ daily [*o.d.*] for 1 day vs. 60 $nmol \cdot kg^{-1}$ *o.d.* for 3 days), and two routes of injection as well (i.v. vs. s.c.), were evaluated through deterministic model-based

simulations. Efficacy of the treatments was expressed as the percentage of reduction with respect the control in the amount of PBG excreted in urine at day four from the start of the phenobarbital challenge.

2.3 | Model building

Figure 1 shows the time profiles of the observations, which together with the current knowledge of the physiology of the heme pathway and the mechanisms of drug action were used to establish the underlying assumptions that support the model structure schematically represented in Figure 2.

2.3.1 | Model for kinetics of PBGD enzymatic activity in serum

Serum profiles of PBGD enzymatic activity were described with a two-compartment model estimating the apparent volume of distribution of the central compartment (V_1), the first order rates constants of

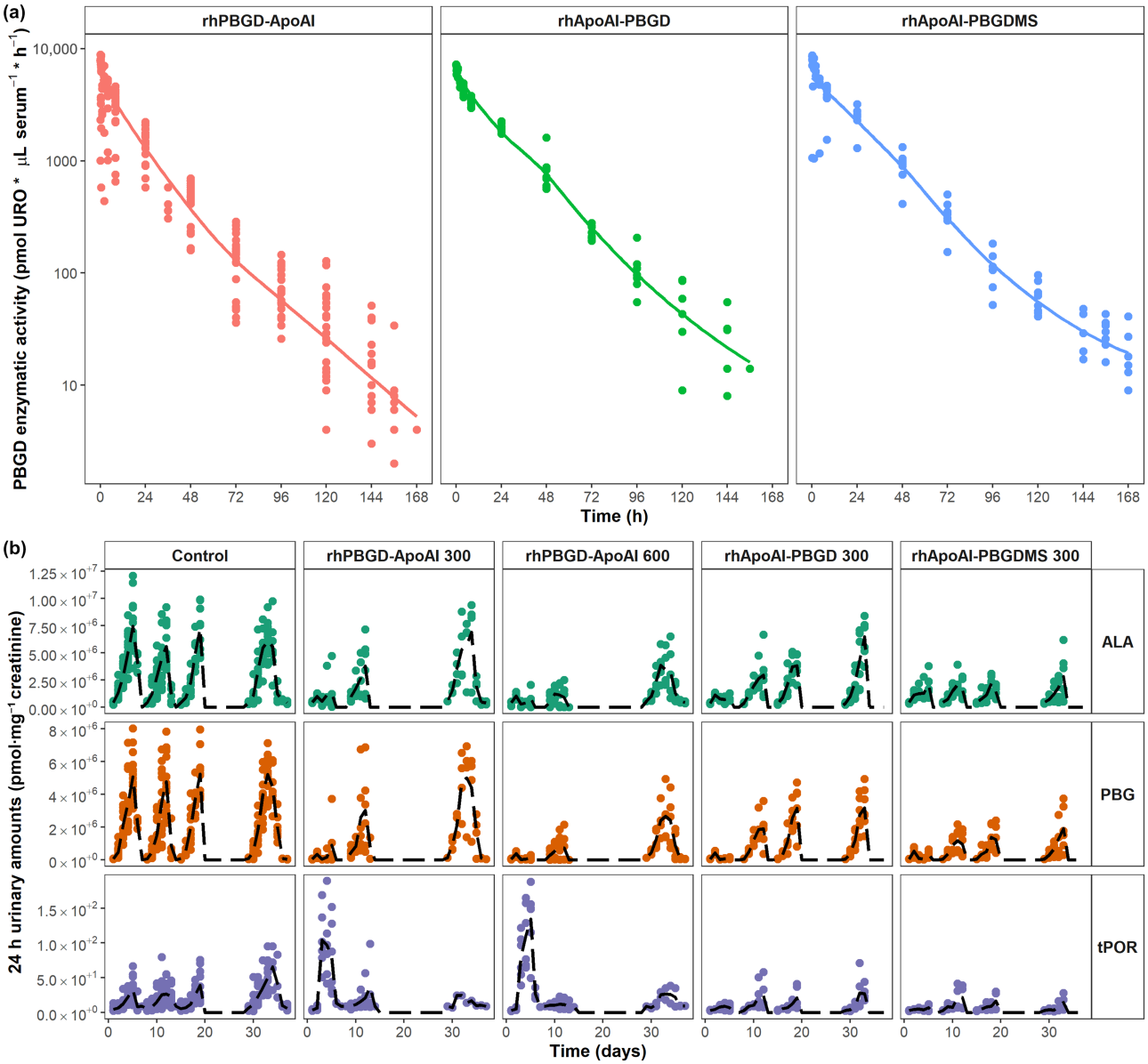

FIGURE 1 Raw data used to build the porphobilinogen deaminase (PBGD) enzymatic activity and heme precursor models. (a) PBGD enzymatic activity profiles over time after a single 60 nmol·kg^{-1} body weight intravenous administration of either recombinant human (rh) PBGD- apolipoprotein AI (ApoAI; $n = 27$), rhApoAI-PBGD ($n = 9$) or rhApoAI-human PBGD-I129M/N340S (PBGDMS; $n = 8$). Points represent the individual activity values, whereas the solid line displays the median tendency. (b) Heme precursor amounts collected in 24 h urine of acute intermittent porphyria (AIP) mice for control ($n = 22$) and treated AIP mice with 300 ($n = 8$) or 600 ($n = 7$) nmol·kg^{-1} body weight of rhPBGD-ApoAI, rhApoAI-PBGD ($n = 7$) or rhApoAI-PBGDMS ($n = 6$). Points show the individual amount values over time, and the dashed line displays the median profile

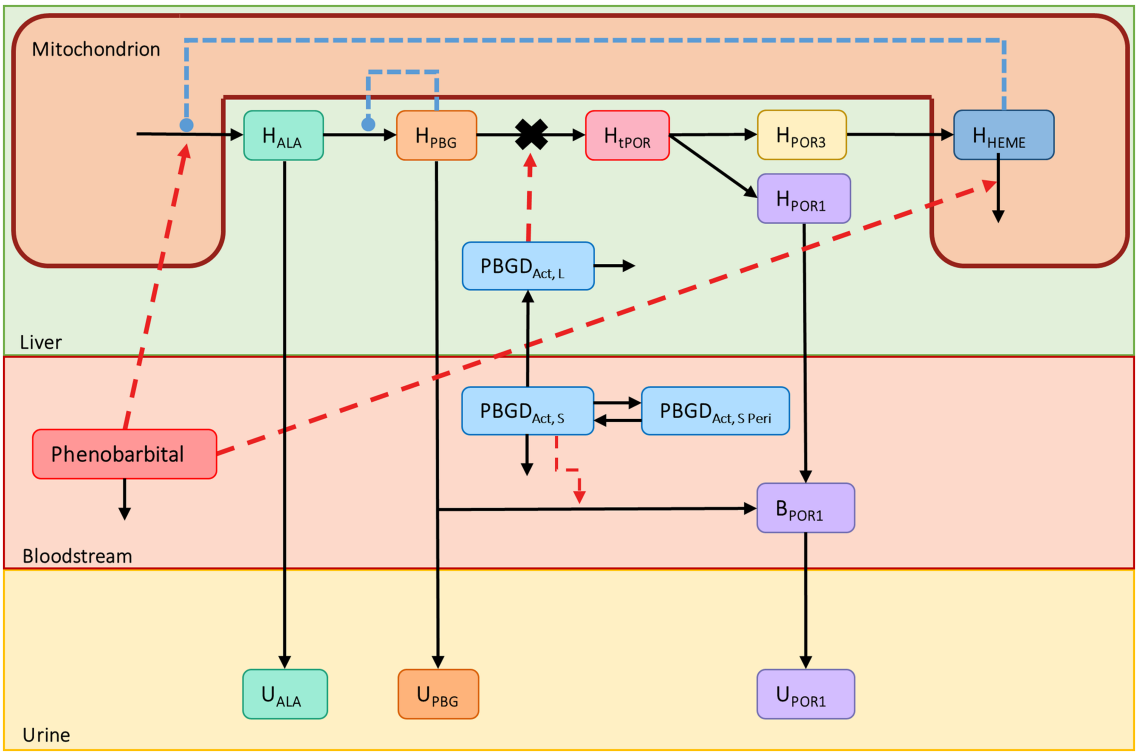

FIGURE 2 Schematic representation of the heme precursors model with porphobilinogen deaminase (PBGD) effects. Black solid arrows represent amount transfers between compartments. Red dashed arrows show stimulation effects from either phenobarbital or PBGD in liver or in the bloodstream. Blue dot-end dashed lines display inhibitory feedbacks from either hepatic heme amounts or hepatic PBG amounts. All the model parameters have been defined in the main text and in the supporting information

distribution between compartments (K_{12} and K_{21}), and a first order rate constant of elimination (K_{el}). To harmonize units between PBGD dose (nmol) and observation (enzymatic activity, pmol URO * μl serum^{-1} * h^{-1}), Apparent volume of distribution of the PBGD enzymatic activity central compartment is expressed as amount/activity.

Differences between PBGD formulations in the pharmacokinetic profiles were tested as covariate effects on each of the model parameters, considering each formulation as a category and rhPBGD-ApoAI being the reference one.

2.3.2 | Heme precursors liver model in the absence of experimental perturbation

Heme is formed in the liver, where ALA is synthesized by ALA synthase (ALAS, EC 2.3.1.37) and then transformed to PBG via ALA dehydratase enzyme (ALAD, EC 4.2.1.24). Subsequently, in the presence of the PBGD enzyme, PBG is transformed to hydroxymethylbilane and then to uroporphyrinogen III by the uroporphyrinogen III synthase enzyme (UROS, EC 4.2.1.75). However, the highly reactive hydroxymethylbilane may cyclize without rearrangement in a nonenzymatic reaction to give uroporphyrinogen I. Uroporphyrinogen decarboxylase catalyse the stepwise decarboxylation of uroporphyrinogen I or II into coproporphyrinogen I or II through the intermediates of hepta-, hexa, and pentacarboxylic porphyrinogens. Isomers I are transferred to blood and excreted via urine predominantly, whereas most of porphyrinogens III continue the pathway until heme is formed (Puy et al., 2010; Phillips, 2019). Although uroporphyrin, the oxidized form of uroporphyrinogen, is mostly excreted as porphyrin, hepta-, hexa-, penta- and coproporphyrins are also detected in urine samples at a lower percentage. Thus, the total porphyrinogens formed from PBG are identified as tPOR, whereas porphyrinogen 1 (POR1) and porphyrinogen 3 (POR3) correspond to porphyrinogens I and III, respectively. Heme levels and its precursors in liver (hepatic, H) H_{Heme}, H_{ALA}, H_{PBG}, and H_{tPOR} were represented in the model by the corresponding compartments with initial conditions defined in the Figure S2. The processes just described are embedded in the set of ordinary differential equations represented by Equations 1–4:

$$\frac{dH_{ALA}}{dt} = K_{enz} \times FDBK_{Heme} - K_{enz} \times FDBK_{PBG \to ALA} \times H_{ALA} \quad (1)$$

$$\frac{dH_{PBG}}{dt} = K_{enz} \times FDBK_{PBG \to ALA} \times H_{ALA} - MM_{PBGD} \times H_{PBG} \quad (2)$$

$$\frac{dH_{tPOR}}{dt} = MM_{PBGD} \times H_{PBG} - K_{enz} \times H_{tPOR} \quad (3)$$

$$\frac{dH_{Heme}}{dt} = K_{enz} \times H_{tPOR} \times (1 - F_{POR1}) - K_{enz} \times H_{Heme} \quad (4)$$

The heme synthesis pathway is a tightly controlled complex biological system which is regulated by feedback (FDBK) and Michaelis–Menten (MM) mechanisms represented in Equations 1–3 by the terms $FDBK_{Heme}$, $FDBK_{PBG\rightarrow ALA}$, and $MM_{PBGD.}$ Where K_{enz} is a rate constant that governs the formation and degradation mechanisms. F_{POR1} is the fraction of formed porphyrinogenc1 out of the total porphyrins formed from PBG (tPOR). A value of 0.909 (90.9%) was assumed in the absence of any treatment due to a higher prevalence of isomer 1 porphyrins in plasma (Hindmarsh et al., 1999) and latter explored through a sensitivity analysis.

Heme, as the final product of the pathway, controls ALA synthesis. This is the most important regulatory mechanism of the entire pathway modelled as shown in Equation 5. Heme decreases the transcription, translation and mitochondria uptake, and also reduces the stability of the mitochondrial ALAS enzyme (Tian et al., 2011), thus reducing ALA production.

$$FDBK_{Heme} = \left(\frac{H_{Heme,0}}{H_{Heme}}\right)^{\gamma_{Heme}} \tag{5}$$

where $H_{Heme,0}$ is H_{Heme} at baseline and γ_{Heme} controls the magnitude of heme inhibition on hepatic ALA synthesis.

A second negative feedback caused by hepatic PBG levels was included in the transit between hepatic ALA and hepatic PBG to account for the steric hindrances on PBGD when there is an excess of PBG (Shoolingin-Jordan & McNeill, 2003) (Equation 6).

$$FDBK_{PBG\rightarrow ALA} = \left(\frac{H_{PBG,0}}{H_{PBG}}\right)^{\gamma_{PBGD}} \tag{6}$$

where H_{PBG0} is H_{PBG} at baseline and γ_{PBGD} is the parameter modulating the effect of the ratio on the transit between hepatic ALA and hepatic PBG.

Finally, AIP is caused by an impaired PBGD activity that limits the formation of hepatic tPOR from hepatic PBG and represented by the Michaelis–Menten expression shown in Equation 7.

$$MM_{PBGD} = \frac{V_{max}}{K_m + H_{PBG}} \tag{7}$$

where V_{max} is the maximum rate of PBG conversion and K_m is the level of hepatic PBG needed to reach half the maximum conversion rate. K_m is derived from the ratio between V_{max} and K_{enz}.

2.3.3 | Heme precursors blood model in the absence of experimental perturbation

As it was the case for liver, systemic levels of heme precursors were not measured. Then levels of ALA and PBG were assumed to be equal to those in liver; thus, $B_i = H_i$, where i refers either to ALA or PBG. Similarly, porphyrinogen 1 in blood, in the absence of treatment, was assumed equal to hepatic exposure, but PBGD therapies may represent an extra source of PBGD enzyme in the serum, resulting in an increase of porphyrin levels in systemic circulation. This is further described below.

2.3.4 | Model for urinary excretion of heme precursors

The amounts of urinary heme precursors excreted in 24 h urine in AIP mice depended on their corresponding non-measured amounts in blood, as shown in Equation 8.

$$\frac{dU_i}{dt} = K_{u,i} \times B_i^{\gamma_i} \tag{8}$$

where U_i is the heme precursor amount measured in 24 h urine, $K_{u,i}$ is the urinary excretion rate constant and γ_i is the parameter modulating the relationship between urinary levels and systemic amounts. The initial condition for U_i is set to zero, assuming a negligible excretion at baseline.

2.3.5 | Model for acute porphyric attacks

Acute attacks were triggered by i.p. administrations of phenobarbital. Concentrations in plasma of phenobarbital (C_{Phe}) were generated considering fast and complete absorption, followed by one compartment disposition properties characterized by an apparent volume of distribution and total clearance of 0.78 L * kg^{-1} and 7.4 $\times$ 10^{-2} L * h^{-1} * kg^{-1}, respectively (Iven & Feldbusch, 1983).

Phenobarbital alters the heme pathway through two different mechanisms: by increasing the hepatic synthesis of ALA, and by decreasing heme deposits as a result of the induced expression of cytochrome P450 (mainly CYP2C9, 2C19 and 3A4i), which in turn triggers the feedback mechanisms $(FDBK)_{Heme}$ regulation mechanism resulting in a delayed inhibition of ALA synthesis. Both effects $E_{Phe,ALA}$ (Equation 9; effect of phenobarbital on ALA synthesis) and $E_{Phe,Heme}$ (Equation 10; effect of phenobarbital on heme degradation) were incorporated in the full model represented in Figure S2.

$$E_{Phe,ALA} = (1 + \theta_{Phe,ALA} \times C_{Phe}) \tag{9}$$

$$E_{Phe,Heme} = (1 + \theta_{Phe,Heme} \times C_{Phe}) \tag{10}$$

$\theta_{Phe,ALA}$ and $\theta_{Phe,Heme}$ are the parameters accounting for the magnitude of phenobarbital effect on ALA synthesis and heme degradation, respectively.

2.3.6 | Model for PBGD effects

The administration of exogenous (E) PBGD promotes the synthesis of porphyrinogen 1 in blood from circulating PBG molecules and it

is thought that it restores PBGD activity in liver. With respect to the former effect, $E_{PBGD,B}$, it was characterized by the following expression (Equation 11) where $\theta_{PBGD,S}$ quantifies the efficiency of the PBG to porphyrinogen 1 reaction process catalysed by exogenous PBGD in serum.

$$E_{PBGD,B} = (\theta_{PBGD,S} \times PBGD_{act,S}) \quad (11)$$

The response to exogenous PBGD in liver follows two mechanisms consisting of enhancing the degradation of PBG to form tPOR represented by $E_{PBGD,L}$ in expression 12, and shifting porphyrin production from porphyrinogen 1 (POR1) to porphyrinogen (POR3), introducing in the model the term F_{POR1}, the fraction of H_{tPOR} corresponding to H_{POR1} (Equation 13).

$$E_{PBGD,L} = (1 + \theta_{PBGD.L} \times PBGD_{act,L}) \quad (12)$$

$$F_{POR1} = \frac{E_{PBGD,L,0}}{E_{PBGD,L} + \theta_{POR1,0}} \quad (13)$$

$\theta_{PBGD,L}$ quantifies the efficiency of the PBG to tPOR reaction process catalysed by exogenous PBGD in the liver, $PBGD_{act,L}$ represents the PBGD activity in the liver scaled from serum as $S_{S\rightarrow L} \times PBGD_{act,S}$ ($S_{S\rightarrow L}$ is a formulation-dependent parameter), $E_{PBGD,L,0}$ is the PBGD activity in liver at baseline and $\theta_{POR1,0}$ is a fixed parameter that allows to obtain a fraction equal to 0.909 in the absence of PBGD treatment.

The full model integrating the processes described in Equations 1–13 is mathematically presented in Figure S2.

2.4 | Software list

Dataset pre-processing and figures were performed with R 4.0.2 (R Foundation for Statistical Computing, 2017) (RRID:SCR_001905) and RStudio 1.3.1073 (RStudio Team, 2020) (RRID:SCR_000432). Berkeley-Madonna 9.1.19 (Park, 2017) was used to test the basic model structure and the different feedback mechanisms. Population approach models were run in NONMEM 7.4 (Beal et al., 2009) (RRID:SCR_016986), and model management and simulations were carried out using Pirana 2.9.9 and PsN 4.9 (Keizer et al., 2013).

2.5 | Materials

Pentobarbital was obtained from. NaH_2PO_4-$2H_2O$, DTT, Cl_2Mg, Tris–HCl (pH 8.1) and TCA from. Duphalyte® was obtained from -Zoetis, Girona, Spain.

2.6 | Nomenclature of targets and ligands

Key protein targets and ligands in this article are hyperlinked to corresponding entries in the IUPHAR/BPS Guide to PHARMACOLOGY http://www.guidetopharmacology.org and are permanently archived in the Concise Guide to PHARMACOLOGY 2021/22 (Alexander, Christopoulos, et al., 2021; Alexander, Kelly, et al., 2021).

3 | RESULTS

3.1 | Data description

The profiles of PBGD enzymatic activity in serum shown in Figure 1a suggested similar kinetics across the different recombinant fusion proteins. Figure 1b shows the time course of the heme precursors for control and treated AIP mice. A reduction of ALA and PBG accumulation in urine is observed after PBGD administration. Urinary ALA and PBG amounts decreased 78–91% and 98%, respectively, with respect to the control group at day 4 (a day after recombinant fusion PBGD dosing). tPOR amounts were reduced as well at day 4 but to a lower percentage (48%–83%) after administering either rhApoAI-PBGD or rhApoAI-PBGDMS, whereas AIP mice in the rhPBGD-ApoAI groups displayed a large tPOR burst during the first phenobarbital challenge (321%–377% increase at day 4 with respect to control group).

3.2 | PBGD enzymatic activity model

The profiles of the systemic PBGD enzymatic activity were best described with a two-compartment model compared with one-compartment kinetics and the use of a three-compartment model did not describe the data significantly better. Including inter-animal variability on the parameters first order rate constant of elimination (K_{el}), apparent volume of distribution of the PBGD enzymatic activity central compartment (V_1) and K_{21} improved the description of the data significantly. The type of formulation showed a significant impact in first order rate constant of elimination, resulting in a 16.2% and 20.8% decrease in first order rate constant of elimination for the rhApoAI-PBGD and rhApoAI-PBGDMS formulations with respect to rhPBGD-ApoAI.

The final model parameters are listed in Table 1. Parameter estimates were precisely estimated with narrow 95% confidence intervals including the parameter value, and the results from the simulation-based diagnostics indicated that the selected model captured well both the typical tendency of the data and their dispersion (Figure 3a). Observed and predictive profiles for several mice chosen at random are represented in Figure 3b showing the good performance of the model at the individual level given the low value of ε-shrinkage. Elimination half-life for rhPBGD-ApoAI, rhApoAI-PBGD and rhApoAI-PBGDMS were 12.84, 15.32 and 16.21 h, respectively. These estimates are reflected by the longer time rhApoAI-PBGD formulations, with respect to rhPBGD-ApoAI, remained in the blood. Inter-animal variability was found to be small for first order rate constant of elimination (10.1% expressed as coefficient of variation, CV), whereas apparent volume of distribution of the PBGD enzymatic activity

TABLE 1 Model parameter estimates of the final PBGD enzymatic activity model

Parameter	Value	95% CI	IAV (RSE [%])
Disposition model			
$K_{el\_PBGD-ApoAI}$ (h)	$5.40*10^{-2}$	$5.02*10^{-2}$ to $5.87*10^{-2}$	10.1 (3.9–14.5)
$K_{el\_ApoAI-PBGD}$ (h)	$4.54*10^{-2}$	$3.81*10^{-2}$ to $5.44*10^{-2}$	
$K_{el\_ApoAI-PBGDMS}$ (h)	$4.26*10^{-2}$	$3.61*10^{-2}$ to $5.04*10^{-2}$	
V_1 (nmol PBGD * µl serum * h * pmol URO^{-1})	$2.97*10^{-4}$	$2.59*10^{-4}$ to $3.48*10^{-4}$	40.2 (15.2–62.5)
K_{12} (h)	$3.68*10^{-3}$	$2.01*10^{-3}$ to $1.06*10^{-2}$	-
K_{21} (h)	$3.52*10^{-2}$	$2.07*10^{-2}$ to $6.51*10^{-2}$	61.3 (23.6–127.9)
Error model (%)	32.9	27–38	-
Absorption model (subcutaneous only)			
K_a (h)	$1.66*10^{-2}$	$1.05*10^{-2}$ to $2.35*10^{-2}$	50.1 (19.5–87.1)
D (h)	15.0	13.6–16.3	-
$F_{1st\ order}$ (unitless)	0.33	0.28–0.42	60.3 (20.5–91.6)
F_{subc} (unitless)	0.94	0.88–0.99	-

Notes: RSE, relative standard error, computed as the ratio between the standard error and the parameter value and expressed as percentage. 95% confidence intervals (CI), 95% confidence intervals obtained after performing a non-parametric bootstrap. IAV, inter-animal variability, expressed as a coefficient of variation in percentage using the expression $\sqrt{e^{\omega_i^2}-1}$. K_{el}, first order elimination rate constant for the three different protein variants PBGD-ApoAI, ApoAI-PBGD and ApoAI-PBGDMS. V_1, apparent volume of distribution in the central compartment. K_{12} and K_{21}, first order rate constants of distribution from the central to the peripheral compartments and vice versa, respectively. K_a, first-order absorption rate constant. D, duration of the zero-order uptake. $F_{1st\ order}$, fraction of the absorbed amount through a first-order process. F_{subc}, bioavailability after s.c. administration.

central compartment ($V_{1)}$ and K_{21} parameters presented larger variability among animals (40.2% and 61.3%, respectively).

3.3 | Full heme precursors/PBGD effects model

The rationale behind the design of this model is detailed in the methods section and is mathematically fully described in Figure S2 and was simultaneously fit to all observed available data (the amounts over time of urinary levels of ALA, PBG and tPOR).

During the first modelling attempts no sustained PBGD effects were achieved, as the model over-predicted the urinary levels of ALA and PBG during the second and further phenobarbital challenges. To improve model performance, the duration of treatment effects was extended by applying the compartment concept effect (Sheiner et al., 1979) and incorporating the following expression (Equation 14) into the final model structure (see Figure S2). Data were described significantly better, and the model inaccuracies were corrected.

$$\frac{dPBGD_{act,S\_e}}{dt} = K_{e0} \times (PBGD_{act,S} - PBGD_{act,S\_e}) \quad (14)$$

where $PBGD_{act,S\_e}$ is the PBGD enzymatic activity in the effect compartment and K_e,0 is the first-order rate parameter which dictates the delay between $PBGD_{act,S}$ and $PBGD_{act,S\_e}$.

The addition of inter-animal variability to any of the model parameters was found to be non-significant. Therefore, the only random-effects parameters in the final model were those corresponding to the residual error for urinary levels of ALA, PBG and tPOR.

From all the parameters of the model, V_{MAX} (maximum rate of PBG conversion) results were poorly identified and its value was obtained thorough a local sensitivity analysis. Our experimental data do not contain information on the estimate F_{POR1}, thus the same approach as the one described for V_{MAX} was followed. The values selected for V_{MAX} and F_{POR1} were 1.5 arbitrary units * h^{-1} and 0.1 (unitless), respectively.

Model parameter estimates, along with their 95% confidence intervals, are displayed in Table 2 and the results of the model evaluation shown as visual predictive checks are represented in Figure 4. Both, the median tendency and dispersion of the data appear well described for each precursor and experimental scenario. Figure S3 shows experimental data and individual model predicted profiles for several mice chosen at random, where are in a good agreement between observations and predictions is observed.

In the absence of PBGD administration (i.e. control AIP mice), the model predicts 2.31 times greater effects of phenobarbital administration on cytochrome P450 induction (and subsequently on heme degradation) compared with those exerted on the direct stimulation of ALA synthesis (Figure 5). Predicted heme concentrations were reduced by 85% after the first phenobarbital challenge. The overall effect of the lowest heme concentration on ALA regulation increased the K_{ENZ} parameter by 16.7% with respect to its value at baseline (0.47 h). Figure 5a shows a simulation of how phenobarbital induction changes hepatic ALA and hepatic heme virtual concentrtions.

The rationale for development of different PBGD formulations relied, at least in part, on the hypothesis that the position of the ApoAI molecule in the fusion protein was a key factor in PBGD

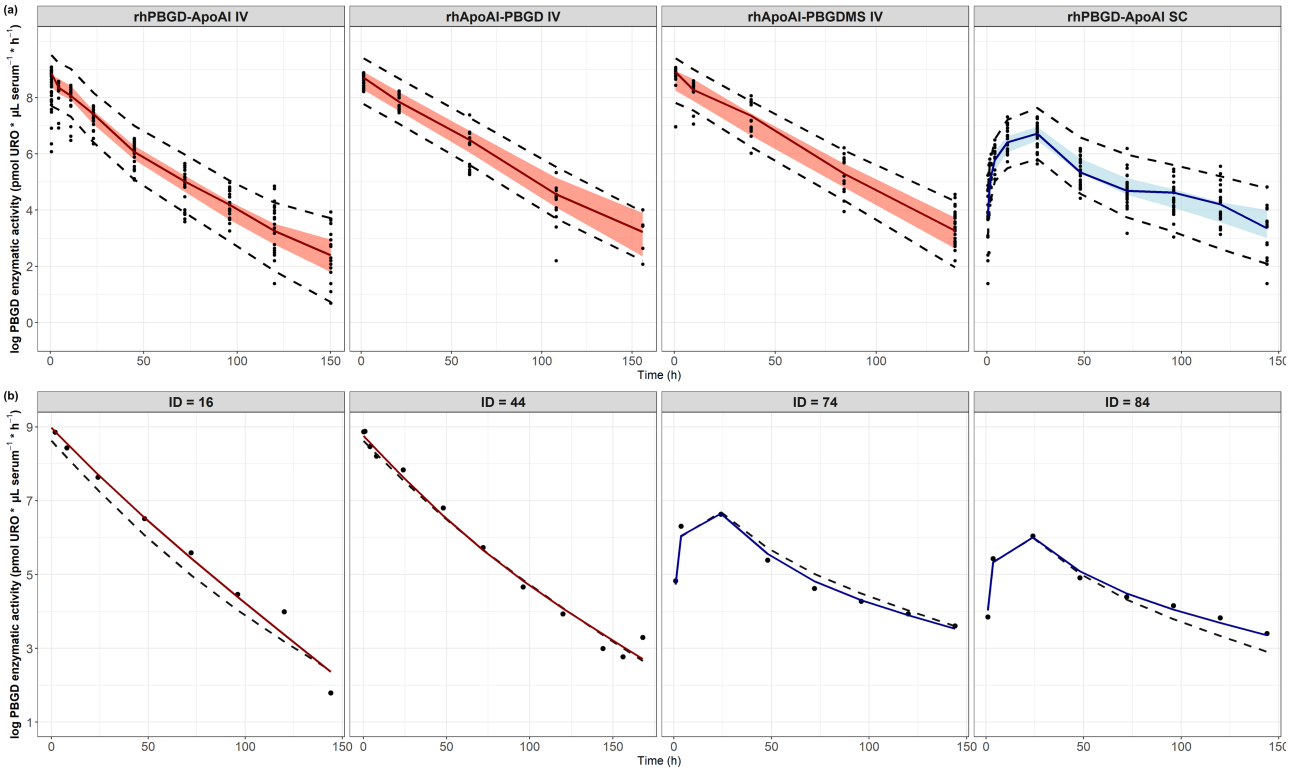

FIGURE 3 Porphobilinogen deaminase (PBGD) enzymatic activity model: Visual predictive checks (VPCs) and individual profiles. (a) VPCs. The three first panels show the different formulations administered intravenously ($n = 27$, 9 and 8 mice, respectively). The fourth panel is for recombinant human (rh) PBGD-apolipoprotein AI (ApoAI; $n = 31$ in total for the four dose groups) after a subcutaneous administration. One thousand datasets with the same characteristics as the original one were simulated and plotted together with the observed data. Points, observations. Red solid line, observed median profile. Light red area, 95% confidence interval of the simulated median profiles. Black dashed lines, medians of the simulated 2.5th and 97.5th percentiles that provide a 95% prediction interval. (b) Individual enzymatic activity profiles from randomly selected individuals. The two panels on the left-hand side present two mice after an intravenous administration, and the remaining two IDs received a subcutaneous administration. Dots, enzymatic activity observations. Blue dashed line, population predictions. Red solid line, individual predictions

distribution to liver. Indeed, in the current analysis different PBGD hepatic uptakes were estimated for each ApoAI position (either rhPBGD-ApoAI or rhApoAI-PBGD). Both rhApoAI-PBGD and rApoAI-PBGDMS shared the same hepatic PBGD uptake (F_{PBGD}) parameter. F_{PBGD} for both rhApoAI-PBGD and rhApoAI-PBGDMS resulted 2.32 times larger than the one estimated for rhPBGD-ApoAI. This meant a larger PBGD uptake in liver for rhApoAI-PBGD and rhApoAI-PBGDMS formulations. Differences in the hepatic PBGD enzymatic activity over time between the different PBGD formulations are displayed in Figure 5b.

After PBGD administration, the maximum total hepatic PBGD enzymatic activity (391 200 pmol URO * µl serum^{-1} * h^{-1} observed for the rhPBGD-ApoAI formulation) increased the V_{MAX} parameter of the saturable Michaelis–Menten transit almost 42-fold with respect to the value at baseline (1.5 arbitrary units * h^{-1}) (see equation for $E_{PBGD,L}$ in Figure S2). This maximum hepatic PBGD activity also changed the F_{POR1} parameter from 0.909 (baseline) to 0.024, meaning a 97% decrease in the formation of porphyrinogen (POR1) and a 972% increase in the formation of porphyrinogen 3 (POR3).

3.4 | External validation

Both the PBGD enzymatic activity model and the heme precursors model were evaluated to assess whether their predictions were still valid under different experimental scenarios (in our case the use of a different route of administration). To this end, data after PBGD s.c. administration were used to validate heme precursor predictions when PBGD is administered s.c. instead of i.v. To accomplish this goal, first the time profiles of systemic PBGD activity needed to be described characterizing the absorption-related parameters, as the disposition parameters were inferred from the i.v. administration experiments.

A total of 31 mice (240 observations) that received different dose levels of rhPBGD-ApoAI (15, 22.5, 30 or 60 nmol·kg^{-1}) were available for the validation analysis of the PBGD enzymatic activity model. The selected model included a simultaneous zero-order and first-order absorption mechanism after a s.c. administration. Absorption parameters are also listed in Table 1. The estimated drug fraction absorbed through a first-order process ($F_{1st\ order}$) was 33.4%, whereas the

TABLE 2 Model parameter estimates of the final full heme precursors/PBGD effects model

Parameter	Value	95% CI
Unperturbed heme precursors model		
K_{enz} (h)	0.47	0.37–0.59
γ_{Heme} (unitless)	$8.08*10^{-2}$	$2.42*10^{-2}$ to 0.16
γ_{PBGD} (unitless)	0.73	0.64–0.85
V_{max} (arbitrary units * h^{-1})	1.5	-
Urinary excretion of heme precursors		
$K_{u,ALA}$ (h)	12 200	10 845–13 655
$K_{u,PBG}$ (h)	1190	815–1554
$K_{u,tPOR}$ (h)	0.23	0.20–0.26
Phenobarbital-induced acute porphyric attacks		
γ_{ALA} (unitless)	1.11	1.02–1.23
γ_{PBG} (unitless)	2.08	1.91–2.30
γ_{tPOR} (unitless)	1.45	1.25–1.70
$\theta_{Phe,ALA}$ (L * mg^{-1})	$2.99*10^{-2}$	$1.91*10^{-2}$ to $4.03*10^{-2}$
$\theta_{Phe,Heme}$ (L * mg^{-1})	$7.23*10^{-2}$	$1.00*10^{-2}$ to $4.19*10^{-1}$
PBGD effects		
$\theta_{PBGD,S}$ (µl serum * h * pmol URO^{-1})	$1.38*10^{-4}$	$5.70*10^{-5}$ to $2.38*10^{-4}$
$\theta_{PBGD,L}$ (µl serum * h * pmol URO^{-1})	$1.03*10^{-4}$	$4.24*10^{-5}$ to $1.63*10^{-4}$
$\theta_{POR1,0}$ (unitless)	0.10	-
$S_{S\rightarrow L,\ ApoAI-PBGD\ and\ ApoAI-PBGDMS}$ (unitless)	2.32	1.75–3.06
K_{e0} (h)	$2.78*10^{-3}$	$2.25*10^{-3}$ to $3.42*10^{-3}$
Residual error model		
ALA error model (log[(pmol * mg $creatinine^{-1}$])	0.748	0.708–0.792
PBG error model (log[(pmol * mg $creatinine^{-1}$])	0.751	0.713–0.792
tPOR error model (log[(pmol * mg $creatinine^{-1}$])	0.799	0.751–0.854

Notes: 95% confidence intervals (CI), 95% confidence intervals obtained after performing a log-likelihood profiling. Abbreviations: ALA, 5-aminolevulinic acid; ApoAI, apolipoprotein A1; B, blood; PBG, porphobilinogen, PBGD, porphobilinogen deaminase; Phe, phenobarbital; POR 1 porphyrinogen 1; tPOR, total porphyrins; URO, uroporphyrin; Ke0., first-order rate parameter which dictates the delay between PBGD activity in serum and PBGD activity in serum for the effect compartment; Ku, is the urinary excretion rate constant for either ALA, PBG or tPOR; S, parameter that transforms exogenous PBGD activity in serum (S) into PBGD activity in liver (L); K_{enz} is a rate constant that governs the formation and degradation mechanisms in liver; $\theta_{Phe,\ ALA}$, parameter accounting for the magnitude of phenobarbital effect on ALA synthesis; $\theta_{Phe,\ Heme}$, parameter accounting for the magnitude of phenobarbital effect on heme degradation $\theta_{POR1,0}$, parameter that allows to obtain a fraction equal to 0.909 in absence of PBGD effect; $\theta_{PBGD,S}$, quantifies the efficiency of the PBG to porphyrinogen 1 reaction process catalysed by exogenous PBGD in serum; $\theta_{PBGD,L}$, quantifies the efficiency of the PBG to tPOR reaction process catalysed by exogenous PBGD in the liver; γ_{ALA}, parameter modulating the relationship between urinary levels and systemic amounts of ALA. γ_{HEME} controls the magnitude of heme inhibition on hepatic ALA synthesis; γ_{PBG}, parameter modulating the relationship between urinary levels and systemic amounts of PBG; PBG; γ_{PBGD} is the parameter modulating the effect of the ratio on the transit between hepatic ALA and hepatic PBG; $\gamma_{tPOR.}$ parameter modulating the relationship between urinary levels and systemic amounts of tPOR. $S_{S\rightarrow L}$, ApoAI-PBGD and ApoAI-PBGDMS, parameter that scales ApoAI-PBGD and ApoAI-PBGDMS activity in the liver coming from serum; V_{max} is the maximum rate of PBG conversion to porphyrins.

remaining 66.6% presented a zero-order uptake. The model showed a total s.c. bioavailability (total subcutaneous PBGD bioavailability, F_{subc}) of 93.5%, meaning that most of the injected PBGD reached the bloodstream. The results showed in the right-hand panels of Figure 3 revealed that the model was indeed supported by data.

Heme precursors model was assessed by including the urinary excreted amounts of ALA and PBG excreted from three mice that were challenged with phenobarbital after two s.c. doses of 300 nmol·kg^{-1} rhApoAI-PBGDMS at days one and two after the first phenobarbital challenge. Only the PBGD enzymatic activity processes regarding absorption and bioavailability were updated, whereas the rest of the parameters remained unchanged. One thousand studies with the same number of treated mice as the original dataset were simulated, and the percentages of reduction in ALA and PBG compared with control mice

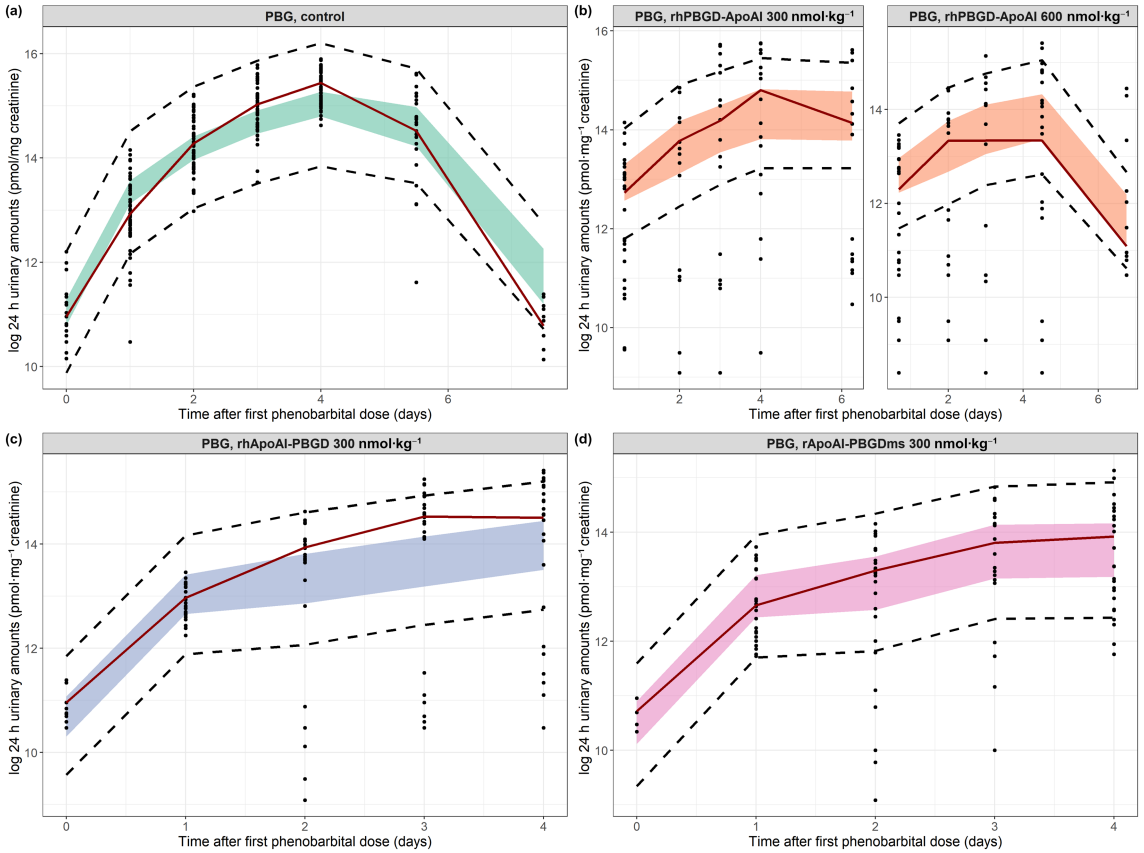

FIGURE 4 Heme precursors model: Visual predictive checks (VPCs). (a) Control ($n = 22$) acute intermittent porphyria (AIP) mice. B, AIP mice treated with either 300 ($n = 8$) nmol·kg^{-1} or 600 ($n = 7$) nmol·kg^{-1} recombinant human (rh) porphobilinogen deaminase (PBGD)-apolipoprotein AI (ApoAI). C, AIP mice treated with 300 ($n = 7$) nmol·kg^{-1} rhApoAI-PBGD. D, AIP mice treated with 300 ($n = 6$) nmol·kg^{-1} rhApoAI-human PBGD-I129M/N340S (PBGDMS). One thousand datasets with the same characteristics as the original one were simulated and plotted together with the observed data. Points, observations. Red solid line, observed median profile. Light areas, 95% confidence interval of the simulated median profiles. Black dashed lines, medians of the simulated 2.5th and 97.5th percentiles that provide a 95% prediction interval

2 days after the second PBGD dose were computed for both observed and simulated data. The observed decrease of ALA amounts in urine (87.1%) was found to be captured by the simulations (95% confidence intervals: 10.4%–94.3%), whereas the observed reduction in urinary PBG levels (99.8%) was represented by the upper part of the 95% confidence intervals calculated from simulated data.

3.5 | Model exploration

Figure 6 shows that the s.c. administration of 300 nmol·kg^{-1} of rhApoAI-PBGDsm can offer an adequate protection (e.g. 80% reduction in the amount of PBG excreted in urine) even if administered up to 7 days prior the start of an acute attack. The degree of protection decreased to 5 days if the same dose is given i.v., and to 3 days if the lower dose of 60 nmol·kg^{-1} is given for three consecutive days both i.v. or s.c. However, if given at the day of the acute attack or later, simulations have shown that s.c. administrations gives equal or less protection than the i.v. route.

4 | DISCUSSION

The development of new therapies for rare diseases is more challenging than for those pathologies that show a higher prevalence in the general population. This is because there is a major obstacle, that of a scarcity information available from such few patients. In that scenario, the possibility of developing predictive computational models by integrating and making the most of the available data represents an attractive goal. Especially, given the current success of the model-informed drug discovery and development paradigm in numerous therapeutic areas (Dockendorf et al., 2018; Garralda et al., 2017; Muliaditan et al., 2017).

Model-based drug discovery and development merges pharmacometrics and systems pharmacology Vicini & Van Der Graaf, 2013). The latter orchestrates data from different sources within a quantitative mechanistic framework following the so-called bottom-up approach. For the particular case of acute intermittent porphyria (AIP), our efforts towards establishing a quantitative systems pharmacology model have been unsuccessful due to

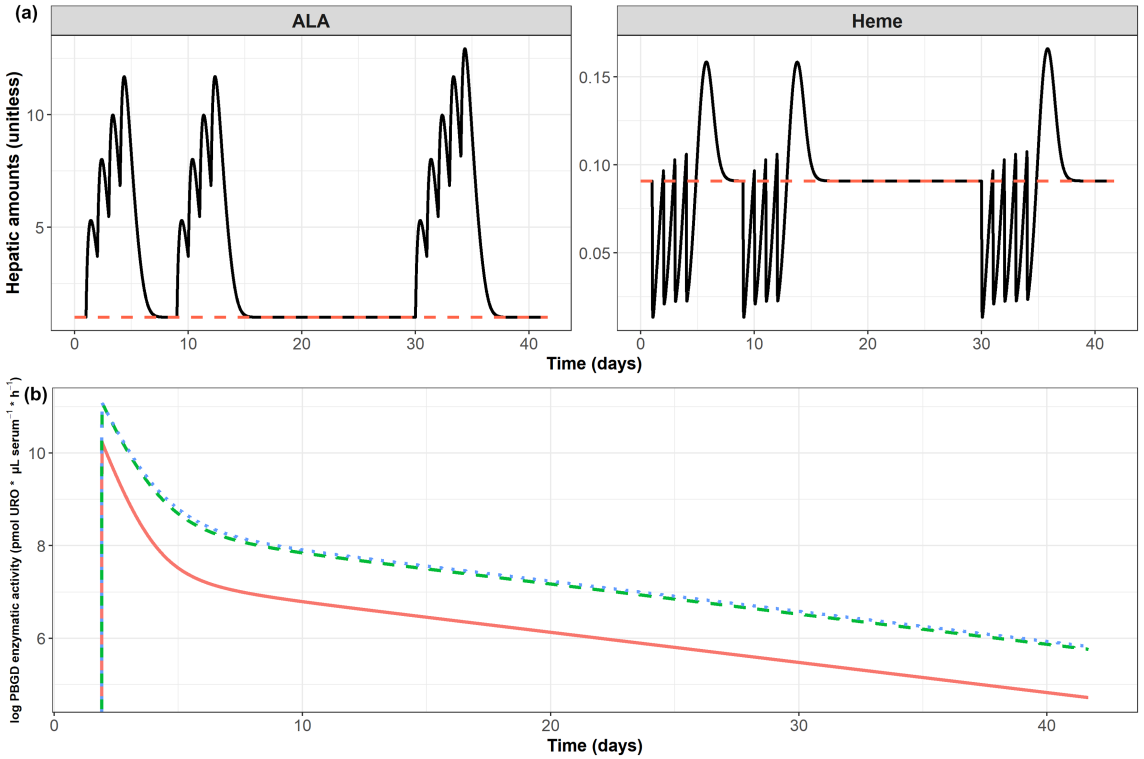

FIGURE 5 Model-based simulated profiles. (a) Hepatic ALA and heme amounts over time with (black solid line) and without (red dashed line) phenobarbital induction, both in the absence of recombinant human (rh) porphobilinogen deaminase (PBGD) administration. (b) PBGD enzymatic activity (expressed as natural logarithm) in liver derived from the administration of 300 nmol·kg^{-1} of either rhPBGD-apolipoprotein AI (ApoAI) (red), rhApoAI-PBGD (green) or rhApoAI-human PBGD-I129M/N340S (PBGDMS; blue)

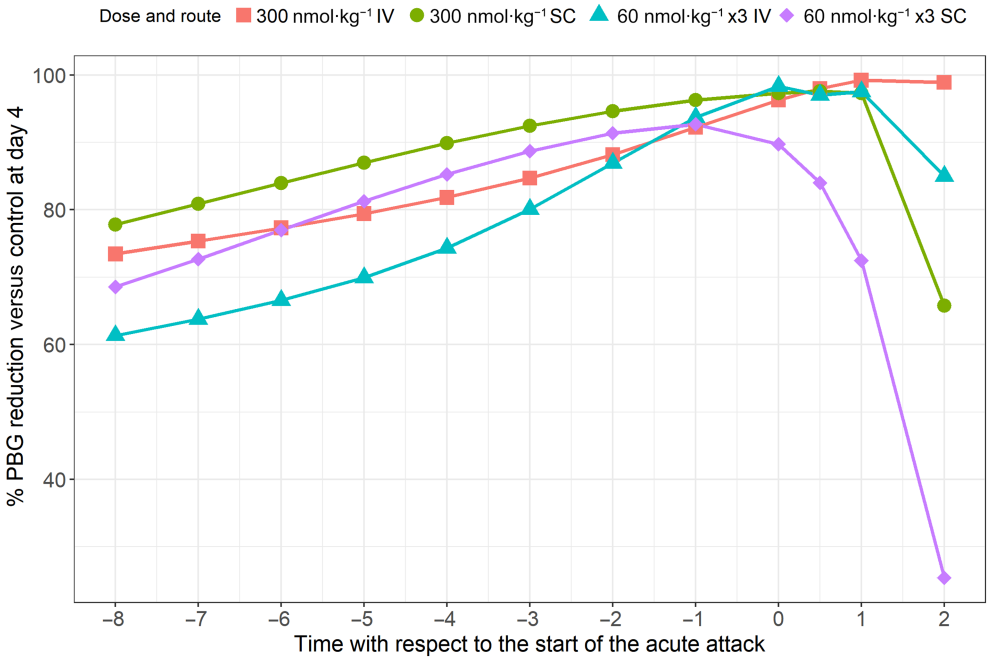

FIGURE 6 Model exploration. Lines represent the percentage of urinary porphobilinogen (PBG) reduced with respect to the control profile at day 4 after the start of the acute attack depending on the day of recombinant human (rh) apolipoprotein AI (ApoAI)- human PBGD-I129M/N340S (PBGDMS) administration: From 8 days prior to the start of the acute attack (day −8) to 2 days after the start of the attack (day 2). Each line shows a different dosing schedule (either 300 nmol·kg^{-1} *o.d.* or 60 nmol·kg^{-1} *o.d.* for 3 days) and route of administration [either intravenous (i.v.) or subcutaneous (s.c.)]

lack of quantitative longitudinal data reflecting key mechanisms of the heme pathway. Therefore, we adopted the intermediate middle-out approach, generating a topological model based on available knowledge (see Figure 2) and the numerical (i.e. parameter characterization) paucity was overcome by a data driven model analysis.

This work represents an extension and a more mechanistic version of the disease progression model established previously in

mice that received phenobarbital but not active treatment (Vera-Yunca et al., 2019). By pooling together data from different experimental groups, we were able to identify and quantify several regulatory processes, such as the inhibition of ALA synthesis by hepatic heme deposits, the inhibition of PBG transit to porphyrins, when there is an excess of this precursor, or the impaired catalytic activity of PBGD in mutated AIP mice. Moreover, the different induction mechanisms that cause an acute attack after a phenobarbital administration have been characterized despite the lack of direct hepatic measurements. The impact of phenobarbital on inducing cytochrome P450 expression (i.e. depleting heme deposits) is more than twice the direct effect on increasing ALA synthesis.

PBGD enzymatic activity model has shown that ApoAI-PBGDMS variants could last longer in systemic circulation. Those formulations presented a 16.2%–20.8% smaller elimination rate with respect to PBGD-ApoAI, which is in agreement with previously obtained internal results that displayed different PBGD kinetics depending on the position of the ApoAI protein. This is also related to the fraction of PBGD in liver: our model describing urinary heme precursor excretion displays a 2.32 times larger hepatic uptake from systemic circulation for rhApoAI-PBGD and rhApoAI-PBGD ms than for PBGD-ApoAI, further confirming that ApoAI position changes PBGD targeting to liver. The larger hepatic uptake of the protein formed by linking ApoAI to the N-terminus of PBGD may be related to its advantaged incorporation into the HDL fraction, as previously suggested (Córdoba et al., 2022).

Additional retrospective data from AIP mice receiving s.c. administrations of PBGD allowed us to characterize PBGD absorption and to confirm that these models were able to describe both PBGD systemic exposure and its effect on heme precursors using different routes of administration. Nevertheless, the model could not entirely predict the percentage decrease of urinary PBG excretion compared with control 2 days after the second PBGD administration. The low number of available mice in this group, only three, may have caused this discrepancy. A larger number of AIP mice with s.c. administrations during an acute attack could help better validate this model.

One of the main applications of mechanistic computational models integrating quantitative longitudinal information from different sources is the exploration of new or alternative dosing scenarios. Several dosing times and routes of administration were tested by performing deterministic simulations in virtual AIP mice. Although s.c. administration proved to be similar to the i.v. route in terms of the prevention of acute attacks (PBG reduction with respect to control mice), its efficacy diminished when the acute attack had already started. In our simulations, rhPBGD exposure achieved by s.c. administration is smaller when compared with i.v. injections, thus showing less efficacy during an ongoing acute attack. However, rhPBGD activity lasts longer and elicited durable protection when administered before an acute attack as shown in Figure S4. This could represent an opportunity for prophylactic treatment of chronic acute attack patients that would not require hospitalization. The rhPBGD therapy could also be divided into three doses of 60 nmol·kg^{-1}, as it gives similar results as the single 300 nmol·kg^{-1}, while reducing the overall rhPBGD amount received.

A previous computational modelling study on AIP showed excellent results regarding the prediction of heme precursors in different preclinical models after PBGD mRNA therapy and the extrapolation of PBGD effects to humans (Parra-Guillen et al., 2020). That semi-mechanistic work had a simpler structure than our mechanistic model, although allowing them to obtain accurate model parameter estimates, to predict key heme precursors amounts in different species and to extrapolate PBGD activity over time to humans. Key parameter estimates were similar to the ones obtained by our model, such as is a rate constant that governs the formation and degradation mechanisms (Kenz; 0.33 vs. 0.47) or urinary excretion rate constants (7600, 1100 and 0.05 vs. 12 200, 1190 and 0.23). Nevertheless, due to the partially empirical nature of this model by Parra-Guillén et al., (i), ALA and PBG dynamics in liver could not be differentiated, (ii) a second PBGD effect was included in the model to decrease ALA synthesis and (iii), drug-mediated induction of the acute attack was directed only to ALA synthesis. In the present work, the time course of each heme precursor (i.e. ALA, PBG and tPOR) can be followed in liver, bloodstream or urine taking into account actual regulatory feedbacks present in the heme pathway. Both inductor (phenobarbital) and recombinant PBGD effects have been mechanistically added as described in literature or in previous works.

In summary, a mechanistic pharmacokinetic-pharmacodynamic (PKPD) model able to capture the urinary time profiles of heme precursors ALA, PBG and tPOR has been successfully developed. It can describe AIP mice biochemical changes during a drug-induced acute attack, and how biomarker levels in urine are restored to normal levels after the administration of recombinant PBGD doses. This model represents a mechanistic framework that can integrate longitudinal, sparse data from multiple sources (e.g. *in vitro* PBGD activity, *in vivo* urinary heme precursor amounts) in order to describe the mechanisms of the heme pathway, acute attack precipitation and treatment effect. Both current and emerging therapies can be included in the model regardless of the dosing schedule to explore their potential for restoring the normal function of the heme pathway.

ACKNOWLEDGEMENTS

DV-Y was supported by a Formación de Profesorado Universitario (FPU, FPU18/01165) grant from the Spanish Ministry of Education. KMC was supported by a grant from a Contrato Predoctoral de Formación en investigación en salud (PFIS, FI19/00014), Spanish Instituto de Salud Carlos III. DJ received a scholarship (F19-010-V) from the Spanish Fundación FEDER para la investigación de enfermedades raras. This study was supported by grants from the Spanish Instituto de Salud Carlos III (FIS) co-financed by European FEDER funds (PI18/00860 and PI21/00546) and Spanish Fundación Mutua Madrileña.

AUTHOR CONTRIBUTIONS

Data were obtained from experiments performed by KMC, DJ and AF. DV-Y, ZPP-G and IFT carried out the data analysis and model building. DV-Y, IFT, AF and ZPP-G wrote the manuscript.

CONFLICT OF INTEREST

The financial sponsors had no role in the analysis or the development of conclusions.

DECLARATION OF TRANSPARENCY AND SCIENTIFIC RIGOUR

This Declaration acknowledges that this paper adheres to the principles for transparent reporting and scientific rigour of preclinical research as stated in the *British Journal of Pharmacology* guidelines for Design and Analysis and Animal Experimentation, and as recommended by funding agencies, publishers and other organizations engaged with supporting research.

DATA AVAILABILITY STATEMENT

The data that support the findings of this study are available from the author Antonio Fontanellas (afontanellas@unav.es) upon reasonable request.

ORCID

Diego Vera-Yunca https://orcid.org/0000-0003-0821-9456
Zinnia P. Parra-Guillen https://orcid.org/0000-0003-1503-2710
Iñaki F. Trocóniz https://orcid.org/0000-0003-3700-8658

REFERENCES

Alexander, S. P., Christopoulos, A., Davenport, A. P., Kelly, E., Mathie, A., Peters, J. A., Veale, E. L., Armstrong, J. F., Faccenda, E., Harding, S. D., Pawson, A. J., Southan, C., Davies, J. A., Abbracchio, M. P., Alexander, W., Al-hosaini, K., Bäck, M., Barnes, N. M., Bathgate, R., … Ye, R. D. (2021). THE CONCISE GUIDE TO PHARMACOLOGY 2021/22: G protein-coupled receptors. *British Journal of Pharmacology*, *178*(S1), S27–S156. https://doi.org/10.1111/bph.15538

Alexander, S. P., Kelly, E., Mathie, A., Peters, J. A., Veale, E. L., Armstrong, J. F., Faccenda, E., Harding, S. D., Pawson, A. J., Southan, C., Davies, J. A., Amarosi, L., Anderson, C. M. H., Beart, P. M., Broer, S., Dawson, P. A., Hagenbuch, B., Hammond, J. R., Inui, K.-I., … Verri, T. (2021). THE CONCISE GUIDE TO PHARMACOLOGY 2021/22: Transporters. *British Journal of Pharmacology*, *178*(S1), S412–S513. https://doi.org/10.1111/bph.15543

Beal, S., Sheiner, L.B., Boeckmann, A., & Bauer, R. J. (2009). NONMEM user's guides. Ellicott City, MD, USA Icon Dev. Solut.

Chen, B., Solis-Villa, C., Hakenberg, J., Qiao, W., Srinivasan, R. R., Yasuda, M., Balwani, M., Doheny, D., Peter, I., Chen, R., & Desnick, R. J. (2016). Acute intermittent porphyria: Predicted pathogenicity of HMBS variants indicates extremely low penetrance of the autosomal dominant disease. *Human Mutation*, *37*, 1215–1222. https://doi.org/10.1002/humu.23067

Córdoba, K. M., Serrano-Mendioroz, I., Jericó, D., Merino, M., Jiang, L., Sampedro, A., Alegre, M., Corrales, F., Garrido, M. J., Martini, P. G. V., Lanciego, J. L., Prieto, J., Berraondo, P., & Fontanellas, A. (2022). The administration of recombinant porphobilinogen deaminase targeted to the liver corrects enzymopenia in acute intermittent porphyria. *Science Translational Medicine*, *14*(627), eabc0700. https://doi.org/10.1126/scitranslmed.abc0700 Epub 2022 Jan 12.PMID: 35020410

Curtis, M. J., Alexander, S., Cirino, G., Docherty, J. R., George, C. H., Giembycz, M. A., Hoyer, D., Insel, P. A., Izzo, A. A., Ji, Y., MacEwan, D. J., Sobey, C. G., Stanford, S. C., Teixeira, M. M., Wonnacott, S., & Ahluwalia, A. (2018). Experimental design and analysis and their reporting II: Updated and simplified guidance for authors and peer reviewers. *British Journal of Pharmacology*, *175*(7), 987–993. https://doi.org/10.1111/bph.14153

Dockendorf, M. F., Vargo, R. C., Gheyas, F., Chain, A. S. Y., Chatterjee, M. S., & Wenning, L. A. (2018). Leveraging model-informed approaches for drug discovery and development in the cardiovascular space. *Journal of Pharmacokinetics and Pharmacodynamics*, *45*, 355–364.

Dover, S. B., Moore, M. R., Fitzsimmons, E. J., Graham, A., & McColl, K. E. L. (1993). Tin protoporphyrin prolongs the biochemical remission produced by heme arginate in acute hepatic porphyria. *Gastroenterology*, *105*, 500–506.

Efron, B. (1992). Bootstrap methods: another look at the jackknife. In *Breakthroughs in statistics* (pp. 569–593). Springer.

Garralda, E., Dienstmann, R., & Tabernero, J. (2017). Pharmacokinetic/Pharmacodynamic modeling for drug development in oncology. *American Society of Clinical Oncology Educational Book*, *37*, 210–215.

Gopal-Srivastava, R., & Kaufmann, P. (2017). Facilitating clinical studies in rare diseases. In *Advances in experimental medicine and biology* (pp. 125–140). Springer New York LLC. https://doi.org/10.1007/978-3-319-67144-4_6

Handschin, C., Lin, J., Rhee, J., Peyer, A. K., Chin, S., Wu, P. H., Meyer, U. A., & Spiegelman, B. M. (2005). Nutritional regulation of hepatic heme biosynthesis and porphyria through PGC-1α. *Cell*, *122*, 505–515.

Hindmarsh, J. T., Oliveras, L., & Greenway, D. C. (1999). Plasma porphyrins in the Porphyrias. *Clinical Chemistry*, *45*, 1070–1076.

Huang, S. M., Abernethy, D. R., Wang, Y., Zhao, P., & Zineh, I. (2013). The utility of modeling and simulation in drug development and regulatory review. *Journal of Pharmaceutical Sciences*, *102*, 2912–2923.

Iven, H., & Feldbusch, E. (1983). Pharmacokinetics of phenobarbital and propylhexedrine after administration of barbexaclone in the mouse. *Naunyn-Schmiedeberg's Archives of Pharmacology*, *324*, 153–159. https://doi.org/10.1007/BF00497022

Jiang, L., Berraondo, P., Jericó, D., Guey, L. T., Sampedro, A., Frassetto, A., Benenato, K. E., Burke, K., Santamaría, E., Alegre, M., Pejenaute, Á., Kalariya, M., Butcher, W., Park, J. S., Zhu, X., Sabnis, S., Kumarasinghe, E. S., Salerno, T., Kenney, M., … Fontanellas, A. (2018). Systemic messenger RNA as an etiological treatment for acute intermittent porphyria. *Nature Medicine*, *24*, 1899–1909.

Kakizaki, S., Yamamoto, Y., Ueda, A., Moore, R., Sueyoshi, T., & Negishi, M. (2003). Phenobarbital induction of drug/steroid-metabolizing enzymes and nuclear receptor CAR. *Biochimica et Biophysica Acta, General Subjects*, *1619*, 239–242.

Karim, Z., Lyoumi, S., Nicolas, G., Deybach, J. C., Gouya, L., & Puy, H. (2015). Porphyrias: A 2015 update. *Clinics and Research in Hepatology and Gastroenterology*, *39*, 412–425.

Keizer, R. J., Karlsson, M. O., & Hooker, A. (2013). Modeling and simulation workbench for NONMEM: Tutorial on Pirana, PsN, and Xpose. *CPT: Pharmacometrics & Systems Pharmacology*, *2*, e50.

Lilley, E., Stanford, S. C., Kendall, D. E., Alexander, S. P., Cirino, G., Docherty, J. R., George, C. H., Insel, P. A., Izzo, A. A., Ji, Y., Panettieri, R. A., Sobey, C. G., Stefanska, B., Stephens, G., Teixeira, M., & Ahluwalia, A. (2020). ARRIVE 2.0 and the *British Journal of Pharmacology*: Updated guidance for 2020. *British Journal of Pharmacology*, *177*, 3611–3616. https://doi.org/10.1111/bph.15178

Marshall, S. F., Burghaus, R., Cosson, V., Cheung, S., Chenel, M., DellaPasqua, O., Frey, N., Hamrén, B., Harnisch, L., Ivanow, F., Kerbusch, T., Lippert, J., Milligan, P. A., Rohou, S., Staab, A., Steimer, J. L., Tornøe, C., & Visser, S. A. (2016). Good practices in model-informed drug discovery and development: Practice, application, and documentation. *CPT: Pharmacometrics & Systems Pharmacology*, *5*, 93–122.

Muliaditan, M., Davies, G. R., Simonsson, U. S. H., Gillespie, S. H., & Pasqua, O. D. (2017). The implications of model-informed drug discovery and development for tuberculosis. *Drug Discovery Today*, *22*, 481–486.

Park, W.-S. (2017). Pharmacometric models simulation using NONMEM, Berkeley Madonna and R. *Translational and Clinical Pharmacology*, *25*, 125–133. https://doi.org/10.12793/tcp.2017.25.3.125

Parra-Guillen, Z. P., Fontanellas, A., Jiang, L., Jerico, D., Martini, P., Vera-Yunca, D., Hard, M., Guey, L. T., & Troconiz, I. F. (2020). Disease pharmacokinetic–pharmacodynamic modelling in acute intermittent porphyria to support the development of mRNA-based therapies. *British Journal of Pharmacology*, *177*, 3168–3182.

Percie du Sert, N., Hurst, V., Ahluwalia, A., Alam, S., Avey, M. T., Baker, M., Browne, W. J., Clark, A., Cuthill, I. C., Dirnagl, U., Emerson, M., Garner, P., Holgate, S. T., Howells, D. W., Karp, N. A., Lazic, S. E., Lidster, K., MacCallum, C. J., Macleod, M., … Würbel, H. (2020). The ARRIVE guidelines 2.0: Updated guidelines for reporting animal research. *PLoS Biology*, *18*(7). https://doi.org/10.1371/journal.pbio.3000410

Phillips, J. D. (2019). *Heme biosynthesis and the porphyrias*. Academic Press Inc.

Puy, H., Gouya, L., & Deybach, J. C. (2010). Porphyrias. *Lancet*, *375*, 924–937. https://doi.org/10.1016/S0140-6736(09)61925-5

R Foundation for Statistical Computing. (2017). R: A language and environment for statistical computing.

RStudio Team. (2020). RStudio: Integrated Development for R.

Schmitt, C., Lenglet, H., Yu, A., Delaby, C., Benecke, A., Lefebvre, T., Letteron, P., Paradis, V., Wahlin, S., Sandberg, S., Harper, P., Sardh, E., Sandvik, A. K., Hov, J. R., Aarsand, A. K., Chiche, L., Bazille, C., Scoazec, J. Y., To-Figueras, J., … Gouya, L. (2018). Recurrent attacks of acute hepatic porphyria: Major role of the chronic inflammatory response in the liver. *Journal of Internal Medicine*, *284*, 78–91.

Serrano-Mendioroz, I., Sampedro, A., Serna, N., de Salamanca, R. E., Sanz-Parra, A., Corrales, F., Berraondo, P., Millet, O., & Fontanellas, A. (2018). Bioengineered PBGD variant improves the therapeutic index of gene therapy vectors for acute intermittent porphyria. *Human Molecular Genetics*, *27*, 3688–3696.

Sheiner, L. B. (1986). Analysis of pharmacokinetic data using parametric models. III. Hypothesis tests and confidence intervals. *Journal of Pharmacokinetics and Biopharmaceutics*, *14*, 539–555.

Sheiner, L. B., Stanski, D. R., Vozeh, S., Miller, R. D., & Ham, J. (1979). Simultaneous modeling of pharmacokinetics and pharmacodynamics: Application to d-tubocurarine. *Clinical Pharmacology and Therapeutics*, *25*, 358–371. https://doi.org/10.1002/cpt1979253358

Shoolingin-Jordan, P. M. L., & McNeill, L. A. (2003). Molecular changes in porphobilinogen deaminase in AIP. *Physiological Research*, *52*, 24S.

Stein, P., Badminton, M., Barth, J., Rees, D., & Stewart, M. F. (2013). Best practice guidelines on clinical management of acute attacks of porphyria and their complications. *Annals of Clinical Biochemistry*, *50*, 217–223.

Syed, Y. Y. (2021). Givosiran: A review in acute hepatic porphyria. *Drugs*, *81*, 841–848.

Thunell, S., Pomp, E., & Brun, A. (2007). Guide to drug porphyrogenicity prediction and drug prescription in the acute porphyrias. *British Journal of Clinical Pharmacology*, *64*, 668–679.

Tian, Q., Li, T., Hou, W., Zheng, J., Schrum, L. W., & Bonkovsky, H. L. (2011). Lon peptidase 1 (LONP1)-dependent breakdown of mitochondrial 5-aminolevulinic acid synthase protein by heme in human liver cells. *The Journal of Biological Chemistry*, *286*, 26424–26430.

Vera-Yunca, D., Serrano-Mendioroz, I., Sampedro, A., Jericó, D., Trocóniz, I. F., Fontanellas, A., & Parra-Guillén, Z. P. (2019). Computational disease model of phenobarbital-induced acute attacks in an acute intermittent porphyria mouse model. *Molecular Genetics and Metabolism*, *128*, 367–375.

Vicini, P., & Van Der Graaf, P. H. (2013). Systems pharmacology for drug discovery and development: Paradigm shift or flash in the pan? *Clinical Pharmacology and Therapeutics*, *93*, 379–381.

Wang, B. (2021). The acute hepatic porphyrias. *Translational Gastroenterology and Hepatology*, *6*, 24.

Zhao, L., Wang, X., Zhang, X., Liu, X., Ma, N., Zhang, Y., & Zhang, S. (2020). Therapeutic strategies for acute intermittent porphyria. *Intractable & Rare Diseases Research*, *9*, 205–216.

SUPPORTING INFORMATION

Additional supporting information may be found in the online version of the article at the publisher's website.

How to cite this article: Vera-Yunca, D., Córdoba, K. M., Parra-Guillen, Z. P., Jericó, D., Fontanellas, A., & Trocóniz, I. F. (2022). Mechanistic modelling of enzyme-restoration effects of new recombinant liver-targeted proteins in acute intermittent porphyria. *British Journal of Pharmacology*, *179*(14), 3815–3830. https://doi.org/10.1111/bph.15821